Journal of Applied Electrochemistry **32**: 1287–1295, 2002.

Electrochemical behaviour of thermally sprayed Cr_3C_2–NiCr coatings in 0.5 M H_2SO_4 media

P.H. SUEGAMA[1], C.S. FUGIVARA[1], A.V. BENEDETTI[1,*], J. FERNÁNDEZ[2], J. DELGADO[2] and J.M. GUILEMANY[2]

[1]*Dep. Físico-Química, Instituto de Química, Universidade Estadual Paulista, UNESP, CP 355, 14801-970 Araraquara, SP, Brazil*

[2]*CPT Thermal Spray Center, Materials Engineering, Dept. Enginyeria Química i Metal-lúrgia, Universitat de Barcelona, C/Martí i Franquès 1. E-08028 Barcelona, Spain*

*(*author for correspondence, e-mail: benedeti@iq.unesp.br)*

Received 21 January 2001; accepted in revised form 30 July 2002

Key words: corrosion, Cr_3C_2–NiCr coating, electrochemical techniques, HVOF, steel protection, thermal spraying

Abstract

The electrochemical behaviour of coated Cr_3C_2–NiCr steel in aerated 0.5 M H_2SO_4 solution was studied by means of electrochemical a.c. and d.c. measurements. A complete structural characterization of the coated steel before and after electrochemical tests was also carried out to access the corrosion mechanism of coated steel, electrolyte penetration through the coating, and to confirm the results obtained using electrochemical techniques. Two types of Cr_3C_2–NiCr coatings produced by a high velocity oxy-fuel spraying system (HVOF) were studied. Differences between coated steels are related to the spraying parameters reflecting their behaviour against corrosion phenomena. The electrochemical behaviour of the coated steel was strongly influenced by porosity and the presence of microcracks in the coating. Once the electrolyte reaches the steel substrate, it corrodes in a galvanic manner resulting in coating detachment from the steel.

1. Introduction

The application of coatings is widely used in industry because of the special properties, which it gives to the substrate. It is also important to note the possibility of obtaining components with mixed and special properties [1, 2].

Thermal spraying processes are considered of great importance in surface technology resulting in an improvement in the quality of resistance, security, and lifetime of many industrial components [3–5]. Rolls, hydraulic systems, valves *etc*., can be coated by means of different thermal spraying processes to obtain an improved surface, which does not fail under extreme working conditions even when submitted to adverse weather conditions [6].

The high velocity oxy-fuel spraying (HVOF) system, which combines the high velocity of a particle of the powder injected into the flame at a relatively high and uniform temperature, seems to be the most competent and feasible of thermal spraying processes against corrosion [7, 8]. The HVOF technique enables processing of materials that are sensitive to oxidation even under atmospheric conditions [9]. This is mainly due to the ability of the particles to reach higher kinetic energy and lower melting degrees, resulting in the flattening of a particle in a plastic state.

To obtain a dense coating, any raw batch, which could be in powder form, is injected into the gun. It is rapidly heated up to a semi-melted state, which is then accelerated and sprayed onto a steel substrate. The spraying of the powder layers produces a coating structure in which it is possible to observe micro- and macrocracks [10–12], pores [13], oxides [14], and different phases generated during the powder melting and rapid solidification [15, 16]. Where coatings resistants against abrasion are needed, these micro- and macrocracks and the heterogeneity of the coating are not of great importance. The problem arises when the coated steel sample must also be resistant against corrosion. Once the electrolyte reaches the steel substrate, galvanic corrosion may occur and the coating is finally detached [17]. Thus, micro- and macrocracks, pores and thermal spraying parameters, are, in general, of great importance when such coatings are subjected to corrosive atmospheres and/or combinations with abrasive/erosive environments.

The Cr_3C_2–NiCr coating is a cermet that combines abrasion resistance and chemical stability of a hard phase (carbides) embedded in a corrosion resistant NiCr matrix. This high chemical stability places it in a good position to obtain a coating with high abrasion resistance, which also offers protection for the steel substrate against corrosive environments.

Some authors have studied the electrochemical behaviour of stainless steel HVOF coatings [17, 18], ceramic coatings such as Al_2O_3 [19] and even some metallic–ceramic combinations such as TiC–NiTi, WC–CoCr, and Cr_3C_2–NiCr [20–22]. Coatings made of 75Cr_3C_2–25NiCr, and 93(WC–Cr_3C_2)–7Ni were also investigated using combined erosion and corrosion tests at room temperature in alkaline and acidic solutions [23]. The mechanism of electrolyte penetration through the coating and main variables that affect the electrochemical behaviour of a cermet coating have still not been clearly explained. Only a few logical trends have been clarified in the study of the corrosion behaviour of such types of system. There are few papers in which it is possible to find complete studies of thermally spray coated steel systems using electrochemical and characterization combined techniques [16, 24].

The aim of the present work is to study Cr_3C_2–NiCr coated steel in an H_2SO_4 solution. The importance of the study of such kinds of coatings in corrosive media is of primary importance in order to substitute hard chromium coatings. There are two problems involved with hard chromium coatings: environmental resulting from their applications, and industrial, caused by their low corrosion resistance [25].

2. Experimental procedure

A commercial Amdry-5420 75Cr_3C_2–25NiCr (wt %) powder was sprayed onto a 42CrMo6 steel substrate (Table 1). Rectangular steel 100 mm × 20 mm × 5 mm samples were degreased and grid-blasted with alumina prior to spraying to obtain a roughened surface (mean roughness around 5 μm) and obtain sufficient cleavage points. Structural characterization of the base steel revealed a ferritic structure with an equiaxial 7–8 μm grain size.

A Sulzer Metco CDS-PT gun was used for high velocity oxy-fuel equipment (HVOF). Mixtures of propylene, oxygen and nitrogen were used as spraying gases and two types of Cr_3C_2–NiCr coatings were deposited using the same sweep rate of the gun, 500 mm s^{-1}. Different spraying parameters are shown in Table 2.

Coating thickness around 253 μm for A and 285 μm for B-coated steels were obtained. The porosity of the samples A and B was estimated by means of the SEM image analysis, using MATROX software. Sample A presented a porosity of (2.5 ± 0.5)% and sample B (1.5 ± 0.5)%. The lower porosity level for coating B was related to the higher energetic flame used which was the main difference between the two coatings evaluated by means of microscopy. Cross-section evaluation of the as-sprayed coatings revealed a homogeneous and well-bounded structure.

Table 1. Chemical composition of the steel substrate (UNS-G11200)

42CrMo6	C	Si	Mn	P	S
wt %	0.22	0.28	0.51	0.02	0.02

Table 2. Spraying parameters used to prepare the samples (studied)

Sample	C_3H_6 /L min^{-1}	O_2 /L min^{-1}	Spraying distance/mm	No. of layers
A	420	60	300	15
B	483	69	200	15

Figure 1 shows the scheme of the electrochemical cell used. A Hg/Hg_2SO_4 $K_2SO_{4,saturated}$ electrode, connected to the solution through a Luggin capillary, was used as a reference electrode and a Pt network was used as an auxiliary electrode and a Pt electrode of small area, connected to the reference electrode by a nonelectrolytic capacitor of 10 μF, was used as the fourth electrode to minimize the ohmic dropping effects and noise [26]. The coated sample was fixed at the bottom of the cell and the exposed geometric area of coated steel was 0.33 cm^2. An electrode made up of the coating without the substrate was prepared by embedding the coating in a polymeric resin with a Pt wire making the electrical contact.

All immersion tests were made using 80 mL of aerated and unstirred 0.5 M H_2SO_4 solution. Open-circuit measurements of the coated steel (E_{OC} against time) were made using EG&G Parc-273 equipment. The sample was tested for around 15 h of immersion in the electrolyte. Coating A without substrate (coating A itself) behaviour was also investigated to compare with the A coated steel.

Electrochemical Impedance measurements (EIS) were made using Solartron-SI1255 equipment and all EIS tests were made after reaching a free electrode potential stability, applying ±5 mV rms and starting from 50 kHz to 1 mHz at 7 points $decade^{-1}$. Frequency response was analysed by means of an electrical equivalent circuit using a program developed by Boukamp [27]. Tafel experiments were then performed using a scan rate of 0.166 mV s^{-1} in a potential range from −100 mV to +350 mV vs E_{OC}.

After the electrochemical measurements, a cross section of both samples was evaluated to confirm the changes in the as-sprayed coated steel and the corroded samples. Structural characterization was determined using an Olympus BH2-UMA optical microscope (OM) and a Topcon SM-300 scanning electron microscope (SEM) coupled to an energy dispersive spectrometer analyser (EDS).

3. Results and discussion

3.1. *Steel, coated steel and coating characterization before and after the tests*

The structural characterization of the steel after a corrosion test showed a homogeneous and deep attack on the sample (Figure 2(a) and (b)). After 20 h of

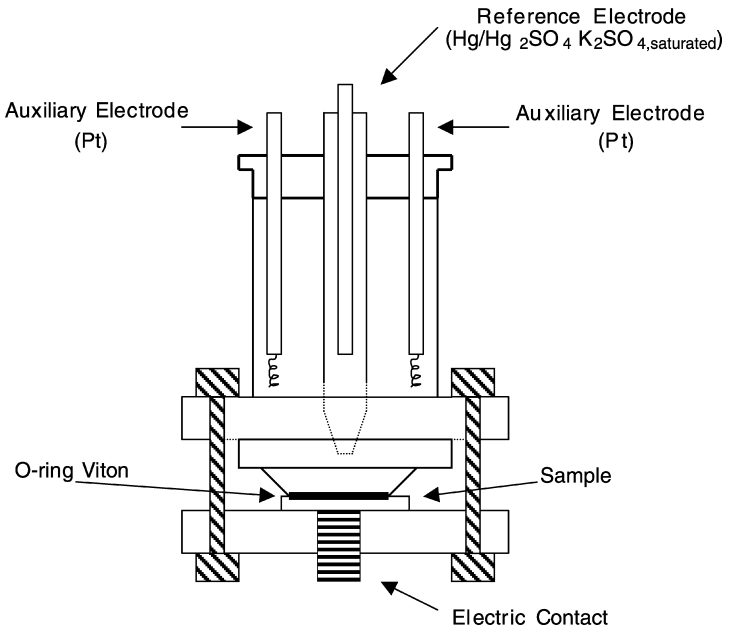

Fig. 1. Scheme of the electrochemical cell.

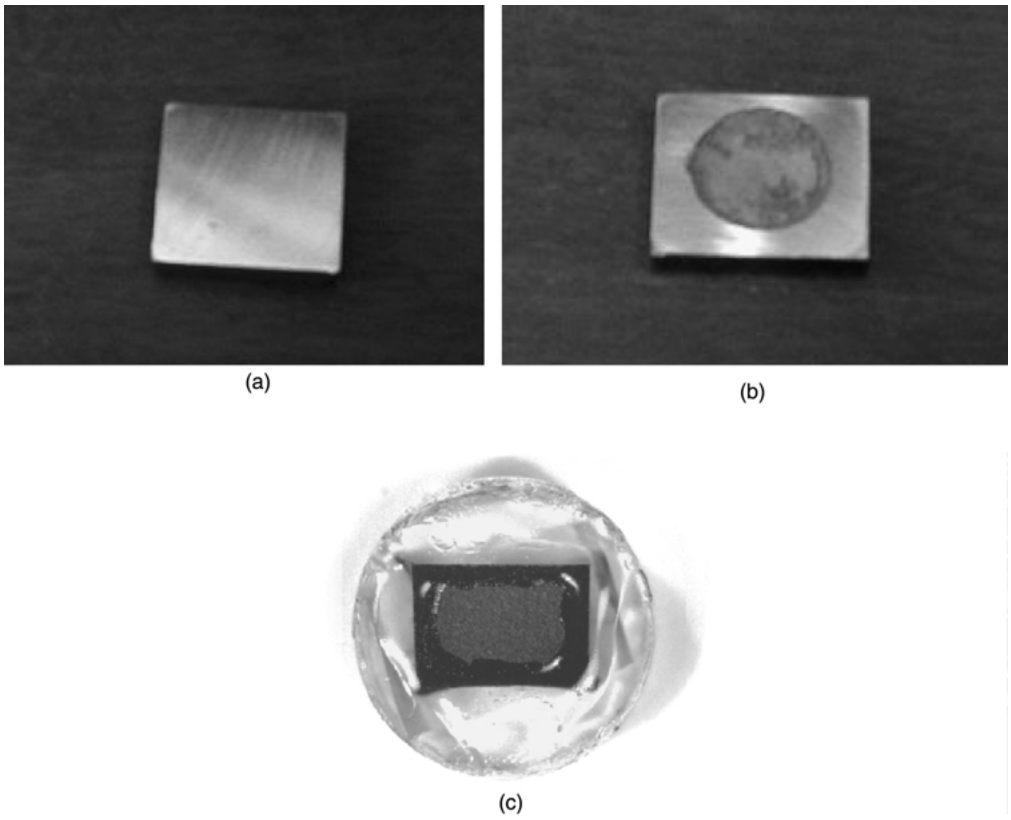

Fig. 2. Top view of the steel before (a) and after 20 h of immersion (b) and A-coated steel after immersion in aerated and unstirred 0.5 M H_2SO_4 solution (c).

immersion the steel substrate was completely corroded and as a result a large amount of Fe salts and oxides was detected on the sample surface after the immersion test. The top view of both coated steels did not suffer any appreciable modification after the same exposure time (Figure 2(c)), since almost the same images were obtained as before the immersion. The Cr_3C_2–NiCr coating did not suffer from this extreme attack and it was noted that few Fe salts and oxides were found at the top of the A- and B-coated steel. Iron salts and oxides were only detected by means of a more sensitive technique. The top view of the coating A itself showed

no appreciable modification after 20 h of immersion in the electrolyte.

As can be seen in Figure 3(a), corresponding to the cross-section structure of the A coating, such systems are composed of a nanocrystalline-NiCr matrix (A) with different percentages of chromium (20–50 in wt %). Carbides such as Cr_3C_2 (B) and either Cr_7C_3 or $Cr_{23}C_6$ were also found, which corresponded to the decomposition process of the initial Cr_3C_2, during spraying. Low Cr_2O_3 (C) content was detected; pores (D), and small cracks (E) appeared between the different deposited layers on both coatings.

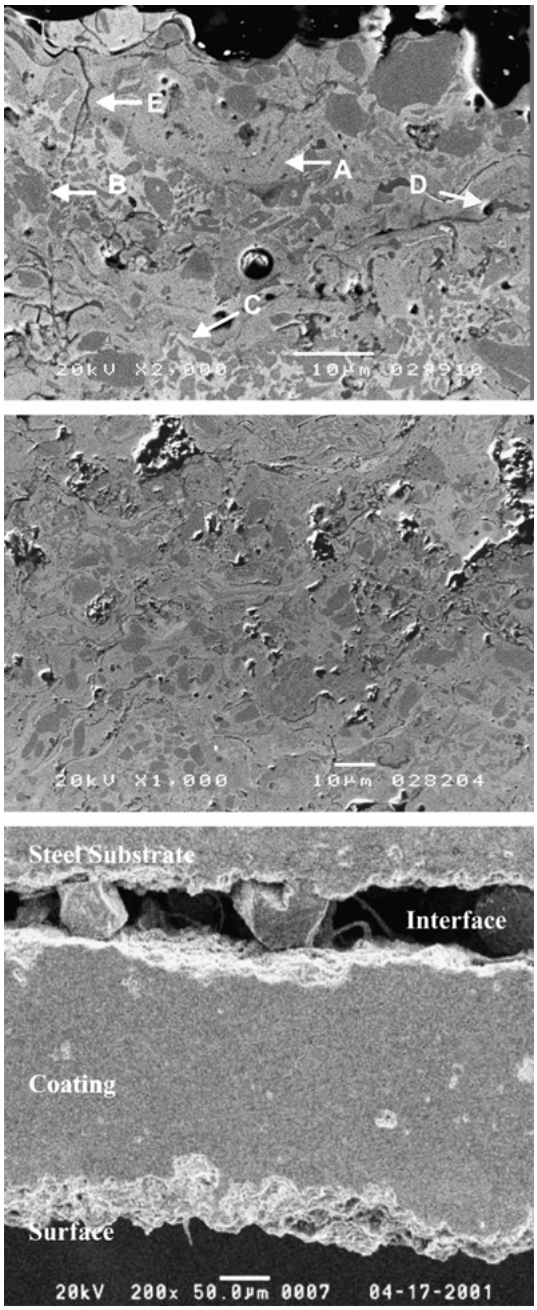

Fig. 3. SEM images of the cross-section for the A-coated steel before immersion (a), and after one month in aerated and unstirred 0.5 M H_2SO_4 (b) and coating detachment from steel after 42 h of immersion and polarization curve (c).

Figures 3(b) and (c) show the coated steel cross-sections of the samples obtained using the A spraying parameters after immersion in a 0.5 M H_2SO_4 solution. After one month of immersion the cross-section showed the presence of a large quantity of pores (Figure 3(b)) and the coating was totally detached from the steel substrate. When the sample was immersed in the electrolyte for 42 h, and submitted to polarization from -0.1 to 0.35 V/E_{OC}, at 0.16 mV s^{-1}, there was a complete detachment of the coating from the steel (Figure 3(c)) and a strong localized attack on the coating was also observed. The B-coated steel showed a similar attack in such an environment, but of minor intensity, delaying the coating-substrate detachment.

After one month of immersion of the coating itself the porosity remained almost the same and a weak localized attack was observed. The SEM characterization revealed a preferential attack on the NiCr matrix localized near the carbides. Once the metallic matrix has been corroded, the carbides are easily pulled down during metallographic preparation of the sample, resulting in large porosity in the attacked samples. Oxides obtained during spraying deposition were also attacked and a large number of small cracks and interlayer separations between different deposited layers were noted. These were attributed to the corrosion of the coating structure and generation of stresses. Therefore, a more open structure was produced, which permitted the electrolyte to go through the coating easily and reach the substrate. In the case of A and B samples, stress was also increased due to the accumulation of Fe oxides and salts formed between the base steel and the attacked substrate.

3.2. *Electrochemical characterization*

3.2.1. *Open-circuit measurements*

Figure 4 shows open-circuit potential against time curves for the steel substrate, A- and B-coated steels and coating A itself. The E_{OC} of the steel after 15 h of immersion in 0.5 M H_2SO_4 solution is around -750 mV, showing a growth trend which corresponds to the accumulation of salts and oxides at the top of the sample produced by the strong corrosion of steel. On the other hand, A- and B-coated steels show a decrease of E_{OC} against time, which is close to the values obtained for the steel substrate. Such a strong decreasing behaviour is typical in the systems where the electrolyte easily reaches the base substrate. After 15 h of immersion, the open-circuit potential values for A- and B-coated steels are around -830 and -815 mV, respectively. The open-circuit potential for the coating A without substrate (coating itself) shows $E_{OC} = -376$ mV after 15 h in 0.5 M H_2SO_4 solution. The stable behaviour of the potential indicates the stability and passive state of the coating in such an environment, far from non-constant or non-stable E_{OC} behaviour for the A- and B-coated steels and uncoated steel. The higher corrosion potential shown by the coating itself is due to the stability of its phase components such as chromium carbides, nickel,

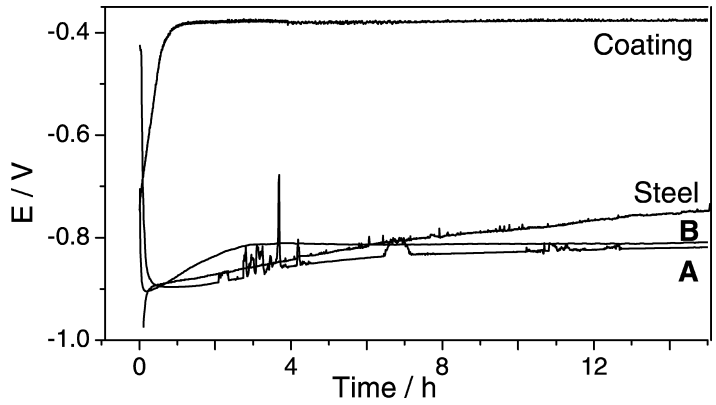

Fig. 4. Open-circuit potential (E_{OC}) against time curves in aerated and unstirred 0.5 M H_2SO_4 solution, at 25 °C.

and chromium oxides, which are nobler than the substrate in A- and B-coated steel.

3.2.2. *Impedance measurements*

Electrochemical impedance spectroscopic (EIS) experiments were performed at the stabilized open-circuit potential, E_{OC}. EIS results for all evaluated systems are shown in Figure 5 (Nyquist plot). Both plots show the experimental (symbol) and simulated (solid line) values using the equivalent circuits (Figure 6) that produced the best fitting (Table 3).

The Nyquist plot for steel (Figure 5) shows a capacitive semicircle that is close to 20 Ω and is the lowest value measured among the systems studied. Two time constants were found and the equivalent circuit that produced the best fitting is shown in Figure 6(a). The R_s value around 15 Ω for all systems studied was related to the solution resistance. The (R_1Q_1) component corresponds to the resistance and the capacitance of the salt and oxide layer formed on the surface of the sample. The second part of the circuit (R_2Q_2) corresponds to the charge transfer resistance and the capacitance of the steel corroded–electrolyte interface. The n values obtained in the fitting were 0.40 and 0.98, respectively, for the first and second components of the equivalent circuit. The value 0.4 suggests an electrolyte diffusion contribution through the salt and oxide layer or a porous electrode. In the case of the steel substrate the porous nature of the salt layer is probably responsible for the n value obtained. An exponential term, n, of the CPE associated with the characteristics of the coating with a value of approximately 0.5 is typical for porous electrodes [28–32]. Similarly, n near 1 is the expected value for a homogeneous and smooth surface [29].

The same equivalent circuit also fitted the impedance data which was obtained for the A- and B-coated steel

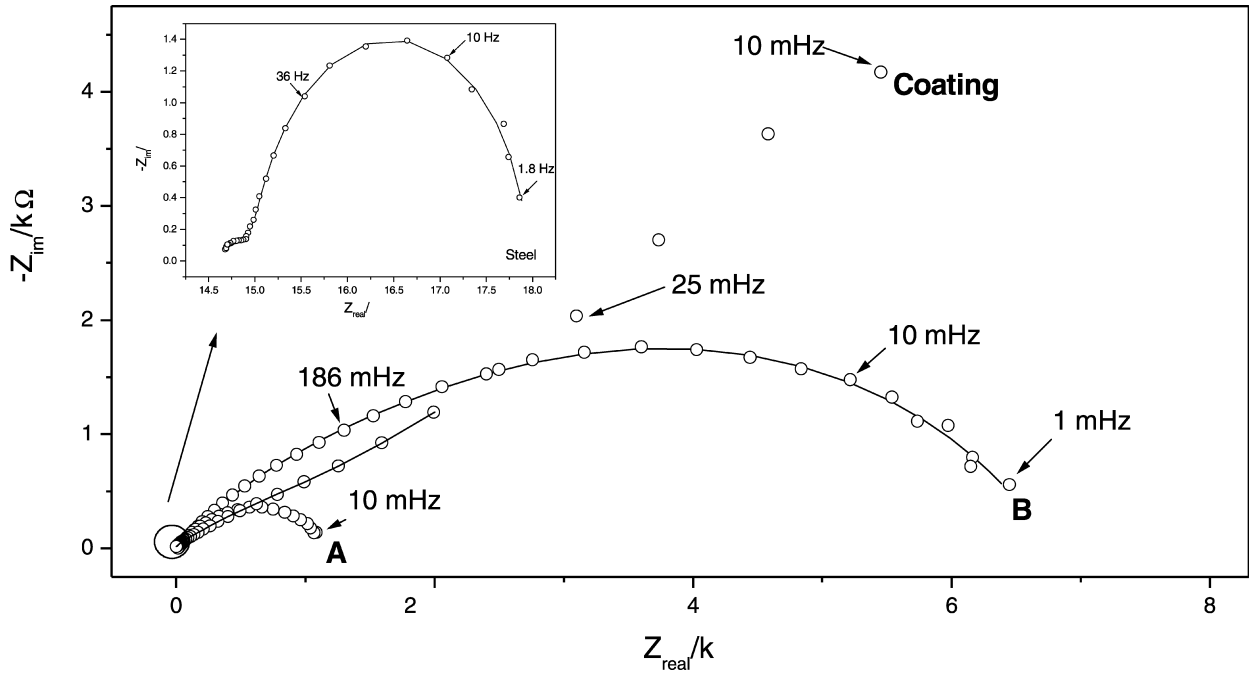

Fig. 5. Experimental (symbol) and simulated (solid line) Nyquist plots for the steel, A- and B-coated steels and coating alone after 15 h of immersion in aerated and unstirred 0.5 M H_2SO_4 solution, at 25 °C.

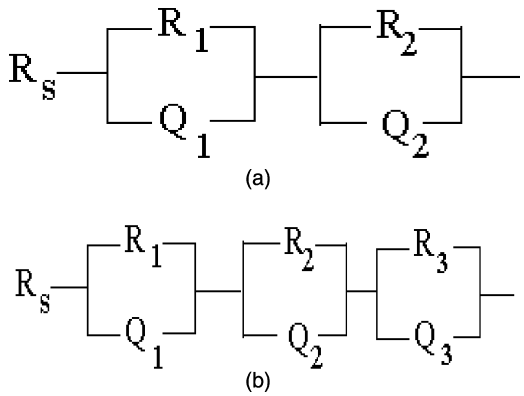

Fig. 6. Equivalent circuits used to fit the impedance data: (a) steel, A- and B-coated steels and (b) coating alone.

very well. Two time constants situated close to 10 Hz and 10 mHz are also observed for the coated steel. The major difference between steel and coated steel corresponds to the phenomenological interpretation of the equivalent circuit components, which is a result of the way that the salt layer on the steel and the coatings A and B were produced. For coated steels, the (R_1Q_1) component was associated to the electrical resistance of the coating and the resistance of the solution in the pores, and Y_{01} to the capacitance of the coating. The (R_2Q_2) is linked to the charge transfer resistance related to the substrate oxidation and Y_{02} to the capacitance of the coated steel–electrolyte electrode. The n value near 0.5 was also associated to the porous nature of the coating, since a porous coating or film containing no diffusional elements mimics the phase angle behaviour of diffusion to a planar electrode [28–32], while an $n = 0.7$ reflects the surface roughness and the high heterogeneity of the coating [33, 34]. As discussed in the characterization section (Section 3.1.1.) the coating shows pores, cracks, and metallic oxides that can be dissolved in the medium, producing interconnected pores and channels responsible for the electrolyte transportation through the coating to the substrate. The coating immersed in the electrolyte behaves similarly to a porous electrode.

In these systems an n value near 0.5 cannot be attributed to oxygen diffusion considering the results obtained for the A-coated steel in both argon and oxygen saturated solutions (Figures 7 and 8). The impedance measurements were made 2 h after immersion in the electrolyte; thus the results were expected to vary in comparison to those obtained after 15 h of immersion. The equivalent circuit that best fitted the impedance results is depicted in Figure 6(a) and the corresponding values of the elements are in Table 4. No significant changes are observed. The R_1 values remained of the same order of magnitude and the R_2 values diminished in the saturated oxygen electrolyte, probably because oxygen accelerated the steel oxidation, after the electrolyte reached the substrate. In both solutions an n value about 0.5 for the element (R_1Q_1) indicated no oxygen diffusion contribution. The n value is probably related to the porous nature of the coating. Therefore, the Y_o and n values had the same explanation as above.

Table 3. Numerical results obtained for the A- and B-coated steels, steel and coating alone using the equivalent circuits showed in Figure 4

	R_1 /Ω	Y_{01} /10^{-3} Ω^{-1} s^n	n_1	R_2 /10^3 Ω	Y_{02} /10^{-3} Ω^{-1} s^n	n_2	χ^2 /10^{-5}			
A	93	6.9	0.49	1.09	0.9	0.69	13			
% error	(0.66)	(15)	(5.8)	(1.5)	(1.5)	(0.91)				
B	2200	0.43	0.58	4.55	1.1	0.71	7			
% error	(0.92)	(3.2)	(6.7)	(1.1)	(23)	(26)				
Steel	0.67	47	0.40	0.003	4.2	0.98	0.3			
% error	(0.44)	(8.1)	(3.4)	(11)	(0.81)	(3.6)				
	R_1 /Ω	Y_{01} /10^{-4} Ω^{-1} s^n	n_1	R_2 /10^3 Ω	Y_{02} /10^{-3} Ω^{-1} s^n	n_2	R_3 /10^3 Ω	Y_{03} /10^{-4} Ω^{-1} s^n	n_3	χ^2 /10^{-5}
Coating	30	4.9	0.65	0.37	1.4	0.63	11.4	9.0	0.85	1.4
% error	(4.5)	(4.7)	(1.1)	(14)	(4.6)	(2.5)	(5.1)	(3.7)	(1.9)	

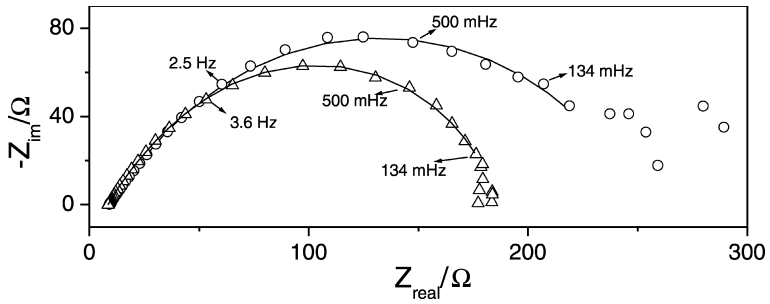

Fig. 7. Experimental (symbol) and simulated (solid line) Nyquist plots for A-coated steel in unstirred 0.5 M H_2SO_4 solution: (○) saturated with argon and (△) saturated with oxygen, at 25 °C. Impedance diagrams recorded 2 h after immersion of the electrode in the electrolyte.

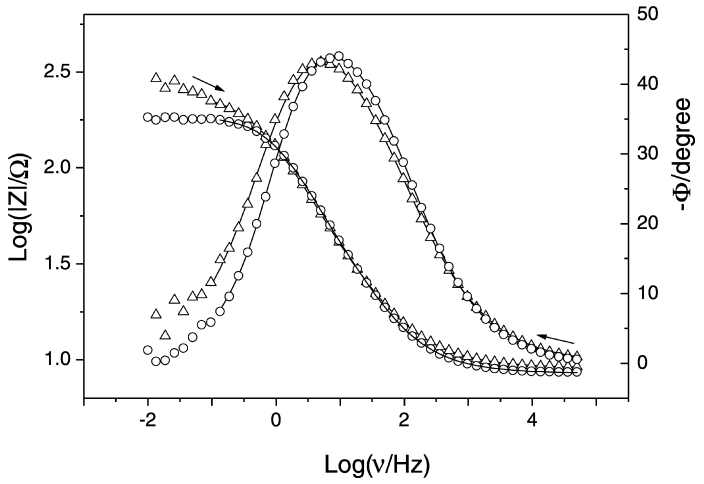

Fig. 8. Experimental (symbol) and simulated (solid line) log $|Z|$ and $-\phi$ against log(f). Bode plots for A-coated steel in unstirred 0.5 M H_2SO_4 solution: (○) saturated with argon and (△) saturated with oxygen. Impedance diagram recorded 2 h after immersion the electrode in the electrolyte.

Table 4. Numerical results obtained for **A** after 2 h of immersion in aerated and deaerated unstirred 0.5 M H_2SO_4 solution using the equivalent circuit in Figure 6

	R_1 /Ω	Y_{01} /10^{-3} Ω^{-1} s^n	n	R_2 /Ω	Y_{02} /10^{-3} Ω^{-1} s^n	n	χ^2 /10^{-5}
Argon	10	7.7	0.54	231	1.6	0.73	7.3
% error	(2.3)	(3.0)	(1.8)	(12)	(4.4)	(0.96)	
Oxygen	37	3.2	0.62	141	1.4	0.85	2.9
% error	(7.3)	(23)	(2.4)	(15)	(23)	(7.1)	

Results obtained for the coating A itself indicated a different behaviour in comparison to the other systems studied. Here at least three time constants were observed. The equivalent circuit depicted in Figure 6(b) fitted the experimental data (solid lines in Figure 5) very well, and the parameters for the elements of the equivalent circuit are shown in Table 3. For the coating A itself the equivalent circuit can be explained as follows: (a) the R_s which was also attributed to the solution resistance; (b) the (R_1Q_1) related to the coating, where R_1 represents the resistances of coating and solution inside the pores, and the Y_{01} was related to the capacitance of the coating; (c) the (R_2Q_2) and (R_3Q_3) parameters were associated to oxygen reduction and NiCr matrix oxidation, respectively, since no steel substrate was present. Several publications about coating corrosion in chloride solutions have attributed the charge transfer reaction to oxygen reduction [21, 35]. It is also well known that the nickel chromium matrix suffers dissolution in sulphuric acid at room temperature, which is accelerated by the anodic polarization [36]. After 15 h of immersion the high R_3 value could be explained by considering the metallic matrix oxidation by the electrolyte. The Y_{02} and Y_{03} reflect the properties of the coating/electrolyte system. A very different corrosion potential for the coating A itself, in comparison to the one measured for the NiCr alloy, was also observed. Coating A itself (Section 3.1.1.) has several different active phases, NiCr being only one of them. The metallic oxides and chromium carbides are nobler then the NiCr alloy, increasing the corrosion potential of the coating A itself.

It can also be noted that R_1 and R_2 values for sample A are higher after 15 h (first line on Table 3) than after 2 h of immersion (Table 4). This may be explained due to the corrosion products such as salt and oxides, which accumulate on the surface and inside the pores, increasing the coating and corrosion resistance.

In the cases of A- and B-coated steels the equivalent circuit which fitted the impedance results better, is simpler than that for coating A itself. For such samples, iron oxidation is the easiest reaction, which presents a lower resistance when compared with that one for the oxidation of coating A itself, but there was higher resistance when compared to the oxygen reduction resistance (Table 3). Therefore, the element (R_3Q_3) in the equivalent circuit (Figure 6(b)) is absent in Figure 6(a) since the iron oxidation dominates the impedance response for A- and B-coated steel.

The charge transfer corrosion resistance for coating A itself is one order of magnitude greater than that of the A- and B-coated steel, and is four orders of magnitude greater than that for the steel substrate.

3.2.3. *Tafel plots*

All Tafel polarization curves recorded after open-circuit potential tests and impedance measurements are shown in Figure 9. These curves were only qualitatively analysed

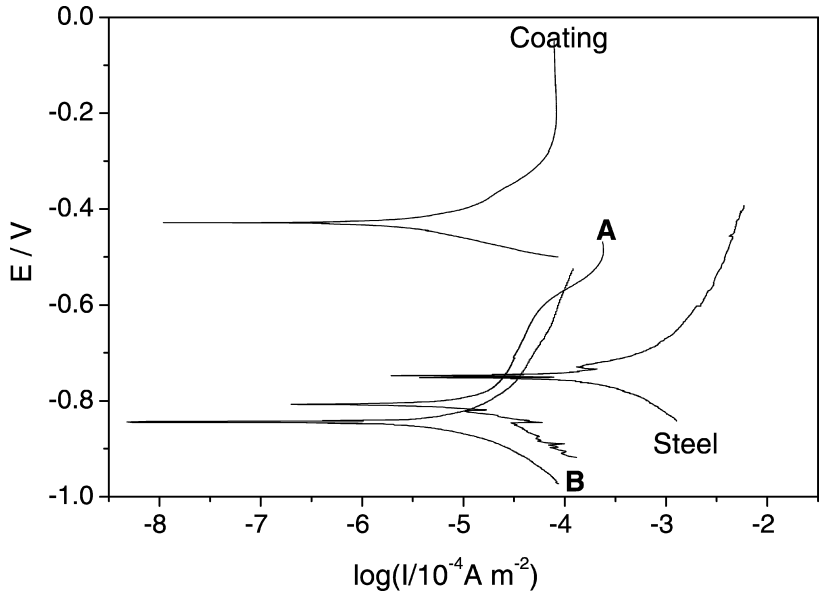

Fig. 9. Tafel plots for all samples in aerated and unstirred 0.5 M H_2SO_4 solution, at 25 °C and $v = 0.166$ mV s^{-1}.

owing to the complex nature of the coated-steel and coating A itself, which leaves no reason to use the Butler–Volmer equation to estimate the Tafel parameters.

The corrosion potential (E_{corr}) estimated from Tafel polarization curves are: (a) −0.75 V for steel; (b) −0.81 V for A-coated steel; (c) −0.83 V for B-coated steel; (d) −0.43 V for coating A and (e) −0.97 V for NiCr alloy [37]. These values agree with those measured in the open-circuit potential tests, thus the E_{OC} values measured after 15 h of immersion (Section 3.2.1.) correspond to the E_{corr}. The presence of nobler phases in coating A itself (Section 3.1.1.) is responsible for the higher E_{corr} value.

The anodic branch of the Tafel polarization curves indicated a defined passive behaviour only for coating A itself and the corrosion current corresponding to the steel substrate is at least around 20 times that for the corresponding coated steel and coating A itself. This is in close agreement with the fact that the steel is partially protected and its dissolution rate is lower than the steel substrate with no thermal sprayed coating. It was also observed that the corrosion current density was almost the same for coating A itself and the NiCr alloy, since the NiCr matrix is the main part of coating A itself that suffers corrosion in an H_2SO_4 solution.

4. Conclusions

Coating protects the base steel during the first steps of immersion, but all the steel coated samples were corroded in a galvanic manner resulting in coating detachment from the substrate after long hours of immersion in 0.5 M H_2SO_4 solution. First, the electrolyte penetrates through cracks and pores and secondly, preferentially attacks, the steel substrate. The NiCr matrix and oxides of the coating seem to be the main drawbacks of such coatings used as steel protective layers. Cracks and pores are responsible for the main electrolyte penetration through the coating.

Spraying parameters strongly influence the corrosion resistance of the coated steel; the more energetic the flame the more dense is the structure, showing fewer cracks and pores, leading to better protection of the steel substrate.

The electrochemical characterization of the two coated samples agrees with the structural characterization. Open-circuit results showed an increasing E_{corr} value for the steel and A- and B-coated steel, which is associated with the steel corrosion, and salt and oxide accumulation on the surface of the sample and/or in the pores of the coating. Coating A itself revealed a higher value which was linked to its nobler behaviour in such an electrolyte.

The equivalent circuit that best fits the EIS results is the same two-term $R_s(R_1Q_1)(R_2Q_2)$ circuit for the steel and A- and B-coated samples. The major difference is found in the phenomenological interpretation of the circuit and the calculated data. While the steel shows a (R_1Q_1) time constant associated with the surface corrosion products, such capacitive and resistance components can be attributed to the electrolyte in the coating pores of the A- and B-coated steels and the n values reveal the porous nature of the electrode. The second (R_2Q_2) time constant found in such systems is associated with the charge transfer of the corrosion reaction. Electrochemical tests for coating A itself revealed a more complex behaviour than that for the A- and B-coated steels.

It is thus concluded that the impedance data give the most efficient description of the electrochemical behaviour of coating A itself and coated steels.

Acknowledgements

The Authors wish to thank the FAPESP-Fundação de Amparo à Pesquisa do Estado de São Paulo (Proc. no. 00/01893-9), CNPq-Conselho Nacional de Desenvolvimento Científico e Tecnológico (Proc. no. 521569/95-8) for the scholarship and financial support for this research. We also wish to show our gratitude to the Generalitat de Catalunya for the financial support for the 2001 SRG00145 Project.

References

1. C. Wasserman, *in* The United Thermal Spray Conference, Düsseldorf 17–19 March (Organised by DVS (German Welding Society) and ASM International, 1995), p. 1, ISBN: 3-87155.653-X.
2. S. Grainger and J. Blunt, 'Engineering Coatings, Design and Application', 2nd edn (Abington Publishing, Cambridge, 1998), 319 pp. ISBN: 1-855-73-369-2.
3. L. Pawlowsky, 'The Science and Engineering of Thermal Spray Coatings', (John Wiley & Sons Ed., 1995), 414 pp.
4. S. Tobe, *in* Proceedings of the 15th International Thermal Spray Conference, Nice 25–29 May (Organised by Commissariat à l'Energie Atomique and ASM International, 1998), p. 3, ISBN: 0-87170-659-8.
5. C.M. Eminoglu, R. Knigth, J. DeFalco and M. Dorfman, *in* the United Thermal Spray Conference, Düsseldorf 17–19 March (Organised by DVS (German Welding Society) and ASM International, 1999), p. 39, ISBN: 3-87155.653-X.
6. F. Ladru, E. Lugscheider, H. Jungklaus, C. Herbst and I. Kvernes, *in* Proceedings of the United Thermal Spray Conference, Indianapolis 15–18 September (Organised by DVS (German Welding Society) and Thermal Spray Society of ASM International, 1997), p. 175, ISBN: 0-87170-618-0.
7. M.R. Dorfman and J.A. Debarro, *in* Proceedings of the 14th International Thermal Spray Conference, Kobe 22–26 May (Organised by High Temperature Society of Japan, 1995), p. 567, ISSN: 1241-3074.
8. P. Siitonen, T. Konos and P.O. Kettunen, *in* Proceedings of the 7th National Thermal Spray Conference, Boston 20–24 June (Organised by Thermal Spray Division of ASM International, 1994), p. 105, ISBN: 0-87170-509-5.
9. E. Lugscheider, C. Herbest and L. Zhao, *Surf. Coat. Technol.* **108** (1998) 16.
10. J.M. Guilemany, J. Fernández, A.V. Benedetti and J. Delgado, *in* Proceedings of the International Thermal Spray Conference, Singapore 28–30 May (Organised by Thermal Spray Society of ASM International, 2001), p. 1165, ISBN: 087170-737-3.
11. J.M. Guilemany, P.L. Cabot, J. Fernández, J.M. De Paco and J. Sánchez, *in* Proceedings of the 5th European Conference on Advanced Materials and Processes and Applications, Maastricht 21–23 April (Organised by Netherlands Society for Materials Science, 1997), p. 771, ISBN: 90-803513-1-8, Vol. 1.
12. T. Rogne, T. Solem and J. Berget, *in* Proceedings of the 1st United Thermal Spray Conference, Indianapolis 15–18 September (Organised by DVS (German Welding Society) and Thermal Spray Society of ASM International, 1997), p. 113, ISBN: 0-87170-618-0.
13. B. Normand, W. Herbin, O. Landemarre, C. Coddet and J. Pagetti, *Mater. Sci. Forum* **291** (1998) 607.
14. M. Dvorak and P. Heimgartner, *in* Proceedings of the 15th International Thermal Spray Conference, Nice 25–29 May (Organised by Commissariat à l'Energie Atomique and ASM International, 1998), p. 95, ISBN: 0-87170-659-8.
15. M. Nakayama, H. Ito, R. Nakamura and M. Toh, *in* Proceedings of the 14th International Thermal Spray Conference, Kobe 22–26 May (Organised by High Temperature Society of Japan, 1995), p. 1063, ISSN: 1241-3074.
16. J. Delgado, 'Fenomenología y caracterización de la resistencia a la corrosión electroquímica en diversos medios agresivos de recubrimientos obtenidos por proyección térmica', PhD Thesis, Barcelona (2001) 516 pp.
17. S. Kuroda, T. Fukushima, T. Kodama and M. Sasaki, *in* Proceedings of the 1st International Thermal Spray Conference, Montreal 8–10 May (Organised by German Welding Society (DVS) and ASM International, 2000), p. 455, ISBN: 087170-680-6.
18. R. Hofman, M.P.W. Vreijling, G.M. Ferrari and J.H.W. Wit, *Mater. Sci. Forum* **291** (1998) 641.
19. P. Siitonen, S.L. Chen, K. Niemi and P. Vuoristo, *in* Proceedings of the International Thermal Spray Conference and Exposition, Orlando 28 May–5 June (Organised by Thermal Spray Division of ASM International, 1992), p. 853.
20. J.M. Guilemany, J. Sánchez and J.M. De Paco, *in* The United Thermal Spray Conference, Düsseldorf 17–19 March (Organised by DVS (German Welding Society) and ASM International, (1999), p. 446, ISBN: 3-87155.653-X.
21. P.L. Cabot, J. Fernández and J.M. Guilemany, *Mater. Sci. Forum* **291** (1998) 667.
22. S. Zimmermann and H. Kreye, *in* Proceedings of the 9th National Thermal Spray Conference, Cincinnati 7–11 October (Organised by Thermal Spray Society of ASM International, 1996), p. 147, ISBN: 0-87170-583-4.
23. D. Toma, W. Brandl and G. Marginean, *Surf. Coat. Technol.* **138** (2001) 149.
24. T. Hodgkiess and A. Neville, *in* Proceedings of the 15th International Thermal Spray Conference, Nice 25–29 May (Organised by Commissariat à l'Energie Atomique and ASM International, 1998), p. 63, ISBN: 0-87170-659-8.
25. J.M. Guilemany and J.A. Calero, *in* Proceedings of the United Thermal Spray Conference, Indianapolis 15–18 September (Organised by DVS (German Welding Society) and Thermal Spray Society of ASM International, 1997), p. 717, ISBN: 0-87170-618-0.
26. D. Garreau, J.M. Saveant and E.S.K. Binh, *J. Electroanal. Chem.* **89** (1978) 427.
27. B.A. Boukamp, Equivalent circuit – Users Manual, version 4.5.
28. R. De Levie, *in* P. Delahay and W. Tobias (Eds), 'Advances in Electrochemistry and Electrochemical Engineering' (Wiley-Interscience, NY, 1967), p. 329.
29. M. Cai and S.M. Park, *J. Electrochem. Soc.* **143** (1996) 3895.
30. D.D. Macdonald, *in* R. Varma and J.R. Selman (Eds), 'Techniques for Characterization of Electrodes and Electrochemical Processes' (John Wiley & Sons, Inc. NY, 1991), p. 515.
31. R. De Levie, *J. Electroanal. Chem.* **281** (1990) 1.
32. S.G. Real, J.R. Vilche and A.J. Arvía, *J. Electroanal. Chem.* **341** (1992) 181.
33. W.H. Mulder and J.H. Sluyters, *Electrochim. Acta* **33** (1988) 303.
34. E.D. Bidóia, L.O.S. Bulhões and R.C. Rocha-Filho, *Electrochim. Acta* **39** (1994) 763.
35. J. Hazan and Ch. Coddet, *Mater. Sci. Forum* **291** (1998) 719.
36. M. Chakravortty, R.K. Paramguru and P.K. Jena, *Hydrometallurgy* **59** (2001) 45.